Machine learning supported sensor fusion based inter-UAV mmWave beamforming system

1st Gia Khanh Tran and Yuya Sugimoto
Department of Electrical and Electronic Engineering (School of Engineering)
Institute of Science Tokyo
Tokyo, Japan
khanhtg@mobile.ee.titech.ac.jp

***Abstract*—This paper proposes a hybrid sensor-fusion framework for resilient mmWave beamforming between UAVs. Due to the strong directionality of mmWave signals, beam alignment is easily degraded by UAV mobility, wind-induced jitter, and GNSS inaccuracy, especially in urban environments. To address this, we combine a high-accuracy Camera/LiDAR perception method for short-range tracking with a GNSS-based approach that is more stable at longer distances, switching between them based on a distance threshold. A link budget analysis highlights the necessity of precise alignment when using directional antennas. Using a co-simulation environment integrating MATLAB/Simulink and Unreal Engine, we show that the proposed hybrid method stabilizes link performance across varying distances and improves average spectral efficiency by 8.5% compared to the Camera/LiDAR-only method. The results demonstrate that hybrid sensing is effective for robust, high-throughput inter-UAV mmWave communication.**

***Index Terms*—inter-UAV, mmWave, beamforming, sensor fusion, machine learning**

I. Introduction

Unmanned Aerial Vehicles (UAVs), or drones, are increasingly vital across applications such as logistics, infrastructure inspection, and public safety. For example, they can rapidly establish temporary communication coverage by forming relay links during disasters or large-scale events where existing networks are overloaded. Drone swarms—multiple UAVs operating cooperatively—are expected to further advance these capabilities by enabling complex, coordinated tasks beyond what a single UAV can achieve. However, such swarm-based operations fundamentally rely on reliable, high-bandwidth, and autonomous inter-UAV communication. Establishing and maintaining these links in dynamic, cluttered urban environments remains a significant technical challenge.

Inter-UAV communication is a core enabling technology for advanced UAV missions. These include deploying aerial platforms to provide wireless connectivity in targeted areas [1], extending and reinforcing existing terrestrial networks [2], and supporting post-disaster surveillance and assessment [3]. However, these applications demand high-precision beam tracking, which poses significant challenges for autonomous UAV systems. Unlike conventional terrestrial links, UAV communications face two major vulnerabilities. (i) Dynamic topology and instability: UAVs move rapidly in three-dimensional space, causing continuous changes in link geometry, while wind-induced jitter can introduce high-frequency disturbances that degrade beam alignment. (ii) Lack of reliable positioning: Conventional beam steering depends heavily on GNSS coordinates, yet in urban or disaster environments, GNSS accuracy is often compromised by NLOS blockage, multipath from surrounding structures, or intentional interference. In this work, we define resilient inter-UAV communication as a system capable of autonomously maintaining high-gain beam directivity by leveraging alternative sensing modalities, even in GNSS-denied or highly dynamic conditions.

Millimeter-wave (mmWave) wireless communication has emerged as a key enabler of high-capacity networks in 5G and beyond [4]. Operating in the 10–100 GHz range, mmWave systems provide substantially wider bandwidths than conventional sub-6 GHz bands, supporting ultra-high data rates and low-latency transmission for applications such as augmented reality, high-definition video streaming, and massive IoT [5]. Despite these advantages, mmWave links face significant challenges, including severe path loss, limited diffraction and penetration, and high sensitivity to blockage from buildings, vehicles, and human bodies [6]. To mitigate these issues, various approaches have been explored: directional beamforming and massive MIMO to overcome high path loss, advanced channel estimation and beam alignment techniques to maintain link reliability in dynamic environments [7], and the use of intelligent reflecting surfaces (IRS) and reconfigurable metasurfaces to enhance coverage and robustness [8]. These advancements are accelerating the adoption of mmWave technology across diverse scenarios, including UAV-based and digital-twin-enabled networks [9]. Moreover, recent outdoor experiments have demonstrated the practical feasibility of integrating mmWave communication into UAV platforms, confirming its promise for high-capacity aerial networks [10].

This paper proposes an inter-UAV communication system capable of achieving high data rates through the use of mmWave links. As discussed earlier, mmWave signals experience severe attenuation and strong directionality, making directional beamforming indispensable. However, this requirement demands precise and continuous alignment between the transmitter and receiver—a challenging task given the high mobility and instability of UAVs. To address this problem, we develop a machine-learning-supported, sensor-fusion-based beamforming algorithm designed to maintain accurate alignment under dynamic flight conditions.

TABLE I
NUMERICAL PARAMETERS FOR LINK BUDGET DESIGN.

Paramater	Value
Center Frequency f_0 [GHz]	from 2 to 60
Bandwidth B	0.5% against f_0
Transmit Power [dBm]	10
Antenna Types	Patch-typed Aperture or Omni
Patch-typed Antenna Size [cm]	10×10
Thermal noise [K]	300
Noise Figure [dB]	10

II. LINK BUDGET DESIGN

Similarly to our study in [9], we aim to design an aerial network that can transfer a data rate of around 0.5 Gbps, facilitating applications such as transferring point cloud data facilitating digital twin construction. Therefore, a simple link budget analysis is conducted as follows.

This study conducts a basic analysis of the propagation characteristics between two UAVs while varying the operating frequency. The system configuration used for the link budget evaluation is shown in Fig. 1, where both UAVs are equipped with aperture antennas directed toward each other. For simplicity, only the direct Line-of-Sight (LOS) path is considered, acknowledging that additional effects such as ground-reflected multipath would further degrade link performance [11]. Under this assumption, the propagation loss between the transmitter and receiver is modeled using the free-space path loss formulation [12].

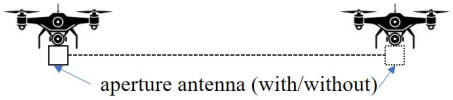

Fig. 1. System model for link budget design.

Figure 1 and Table I summarize the scenarios and system parameters assumed in the numerical analysis. For general analysis, we consider candidate frequencies f_0 ranging from 2 GHz up to 60 GHz, not taking into account regulation issues. For a fair comparison, the bandwidth is scaled against the center frequency with a factor of 0.005 (0.5$\dot{\%}$) such that the bandwidth of a 2 GHz system is 10MHz. We assume that a UAV can be equipped a patch-typed aperture antenna for achieving high directivity, knowing that the size of the square antenna is fixed at $l = 10$ [cm] on each side for a fair comparison. Therefore, the antenna gain G in dB can be calculated as follows [13].

$$G[\mathrm{dB}] = 10 \log_{10} \left(\frac{4\pi \epsilon l^2}{\lambda^2} \right). \tag{1}$$

Here ϵ denotes the antenna's efficiency, $\lambda = \frac{c}{f_0}$ is the wavelength and $c = 3 \times 10^8$ represents the light speed measured in [m/s]. In this study, we evaluated the throughput between the two UAVs by varying their separating distances and the selected center frequencies. The antenna efficiency used in the calculation is $\epsilon = 0.5$ [14].

The propagation loss L_{free} between the two UAVs is assumed to follow Friis' theorem of free space path loss, and can be computed as follows,

$$L_{\text{free}}[\mathrm{dB}] = 20 \log d + 20 \log f_0 + 20 \log \frac{4\pi}{c}, \tag{2}$$

where d represents the distance between the two UAVs. The received power P_{r} at the UE is calculated by

$$P_{\mathrm{r}}[\mathrm{dBm}] = P_{\mathrm{t}} + G_{\mathrm{t}} + G_{\mathrm{r}} - L_{\text{free}} - L_{\text{add}}, \tag{3}$$

where $P_{\mathrm{t}}[\mathrm{dBm}]$ denotes the transmit power from the UAV antenna, G_{t} and G_{r} respectively represents the antenna gains at the UAVs' transmitter (Tx) and receiver (Rx) antennas, computed based on (1). Also, $L_{\text{add}}[\mathrm{dB}]$ denotes excessive loss due to atmospheric absorption as modeled in [15]. From the obtained received power $P_{\mathrm{r}}[\mathrm{dBm}]$, the received power in W is converted as $\sigma_{\mathrm{s}}^2[\mathrm{W}] = 10^{\frac{P_{\mathrm{r}}}{10}-3}$, based on which the communication throughput C in [bps] is calculated using Shannon's theorem as follows.

$$C = B \times \min \left(\log_2 \left(1 + \frac{\sigma_{\mathrm{s}}^2}{\sigma_{\mathrm{n}}^2} \right), \Gamma_{\max} \right). \tag{4}$$

Here B [Hz] is the system bandwidth, $\Gamma_{\max}$ in [bps/Hz] is the maximum value of frequency utilization efficiency determined by the maximum modulation method, and it is assumed that a constellation size of up to 1024 Quadrature and Amplitude Modulation (QAM) is used, i.e. $\Gamma_{\max} = 10$ in this paper. $\sigma_{\mathrm{n}}^2[\mathrm{W}]$ denotes the power of the noise at the receiver. The noise at the receiver is mainly due to thermal noise, and a noise figure of NF $= 10$ is assumed in this paper. In addition, thermal noise can be calculated at room temperature of $T = 300K$ as follows,

$$\sigma_{\mathrm{n}}^2[\mathrm{W}] = k_{\mathrm{B}} B T \times \mathrm{NF}, \tag{5}$$

where k_{B} denotes the Boltzmann constant.

The numerical results are presented in Fig. 2, where the x-axis represents the separation distance between the two UAVs, the y-axis indicates the operating frequency, and the color map shows the achievable throughput. The target performance level is an achievable rate of 500 Mbps. Figs. 2(a) and 2(b) illustrate the case in which only one UAV is equipped with a patch-type directional antenna while the other uses an omnidirectional antenna, whereas Figs. 2(c) and 2(d) correspond to the scenario where both UAVs employ directional antennas. Additionally, Figs. 2(a) and 2(c) show the idealized performance assuming fixed UAV positions with no beam misalignment, while Figs. 2(b) and 2(d) depict the practical case in which UAV locations fluctuate due to environmental disturbances [10], resulting in beam misalignment and an estimated 10 dB gain loss per directional antenna [16], [17].

We first consider the scenario in which only one UAV is equipped with a directional antenna. As shown in Fig. 2(a), the target throughput of 500 Mbps can be achieved only at higher frequencies (e.g., above 10 GHz) due to the increased available bandwidth. The communication range reaches approximately

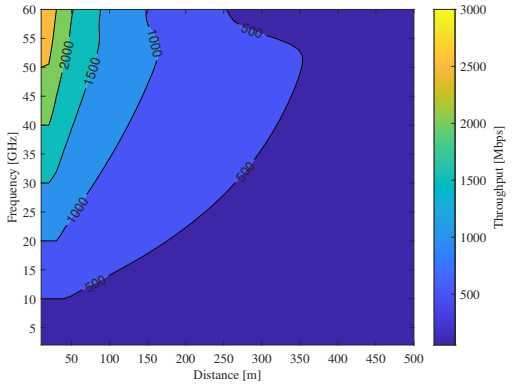

(a) Static, one side

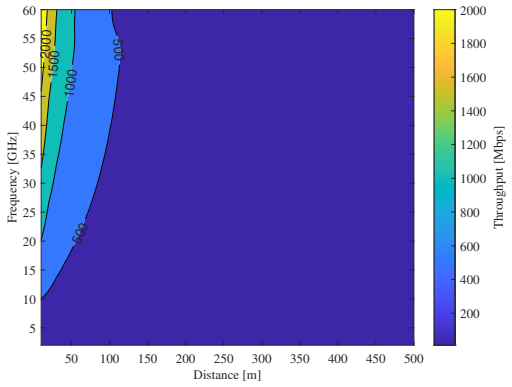

(b) Dynamic, one side

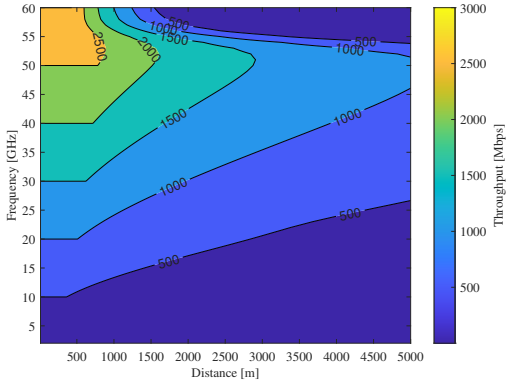

(c) Static, two side

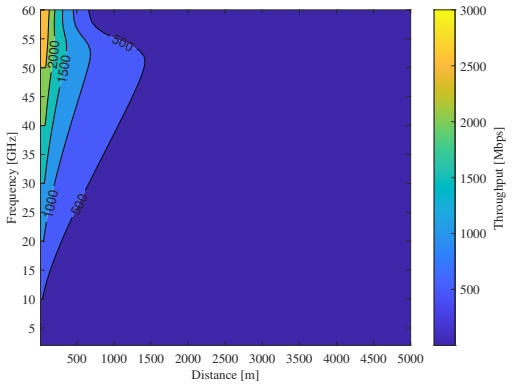

(d) Dynamic, two side

Fig. 2. UAV-UAV link budget design.

350 m when operating near 50 GHz, although this range decreases at even higher frequencies because of atmospheric absorption [18]. However, this represents an optimistic case, as real UAVs experience continuous positional fluctuations caused by wind and other disturbances [10]. Consequently, Fig. 2(b) presents the more pessimistic scenario in which beam misalignment introduces additional gain loss. Under these practical conditions, the maximum communication distance is drastically reduced to around 100 m.

To address the limitations of the single-directional-antenna case, we next consider the scenario where both UAVs are equipped with directional antennas. Figs. 2(c) and 2(d) respectively show the idealized performance with fixed UAV positions and the practical performance when positional fluctuations cause beam misalignment. Although this configuration requires a more complex beam-matching procedure, Fig. 2(d) demonstrates that the achievable communication range can be extended to approximately 1,400 m even under practical conditions when both transceivers employ directional antennas.

III. Machine Learning Based Sensor Fusion Method Facilitating Beam Alignment

Owing to the aforementioned discussion, this section presents our proposed machine learning based sensor fusion method facilitating beam alignment to reduce performance degradation of mmWave communication links. Our primary proposed method is an autonomous, low-latency, and high-accuracy detection and beamforming system that fuses camera and LiDAR sensing. However, its performance is inherently constrained by the camera's detection capability, which degrades when the target UAV is too distant or when image resolution is insufficient. As a result, our earlier work [19] focused only on short-range scenarios within the camera's effective detection range. To overcome this limitation, we introduce a hybrid approach that supplements the short-range Camera/LiDAR method with GNSS-based tracking for long-range operation. As discussed previously, GNSS suffers from a low update rate, which can produce large tracking errors at close range—often exceeding the half-power beamwidth (HPBW) of a narrow, high-gain beam, particularly for fast-moving UAVs. In contrast, the Camera/LiDAR method provides highly accurate angular estimation at short distances. At longer distances, however, the Camera/LiDAR approach reaches its detection limit, whereas the angular error of the GNSS method decreases with range, making it more likely to remain within the beam's HPBW and thereby producing more reliable beam alignment.

Figure 3 illustrates the proposed hybrid beamforming framework. The two UAVs first estimate their relative distance using GNSS. It is assumed that location information is shared via a dedicated, low-rate control channel (e.g., Sub-6 GHz). This channel is assumed to operate independently of the directional mmWave link, enabling the reliable exchange of coordinate information. Although GNSS measurements can exhibit substantial positioning errors [20], this is not critical here because the distance is used solely for determining which sensing method

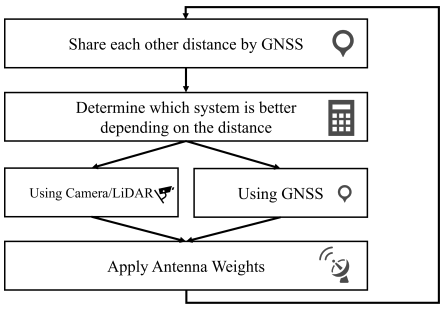

Fig. 3. Diagram of hybrid system model.

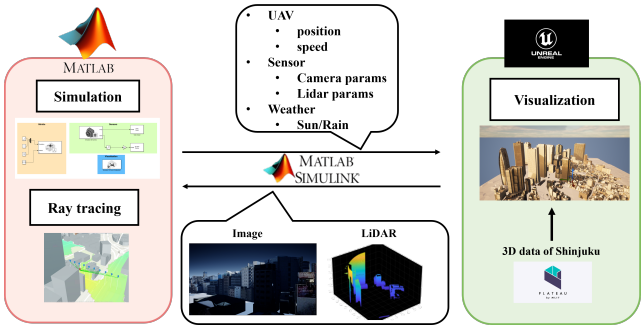

Fig. 4. Simulation Environment.

to activate. When the inter-UAV distance exceeds a predefined threshold, the system relies on the GNSS-based method, as the corresponding angular error remains within the antenna's half-power beamwidth (HPBW). Once the distance falls below the threshold, however, GNSS-induced angular errors become too large for accurate narrow-beam tracking, prompting a switch to the high-accuracy Camera/LiDAR method. The position obtained from the selected sensing modality is then used to compute the antenna weights for beamforming.

The optimal switching threshold could, in principle, be dynamic, given that the HPBW varies with antenna gain. However, the threshold must also consider the physical detection limits of the camera. For practicality, a fixed threshold based on the camera's maximum effective range is often appropriate, regardless of the antenna configuration.

Conventional handover mechanisms are predominantly reactive, initiating only after certain trigger conditions are met during the Time-to-Trigger (TTT) period [21]. To enhance Quality of Service (QoS), proactive handover methods leveraging historical data through machine learning have been proposed [22]. Unlike SNR-based reactive switching—which may occur only after noticeable link degradation—distance-based switching addresses the root cause of beam misalignment, enabling more robust and timely decision-making.

IV. Simulation Setup

A. Simulation Environment

To evaluate the proposed method, we developed a high-fidelity co-simulation environment that integrates MATLAB/Simulink with Unreal Engine (UE), as illustrated in Figure 4. In this environment, a detailed 3D model of Shinjuku, Tokyo, is rendered in UE to produce realistic camera and LiDAR sensor data. These sensor outputs are passed to MATLAB/Simulink, which executes the proposed perception and beamforming algorithms and performs ray-tracing–based mmWave propagation analysis. This co-simulation framework enables precise and comprehensive performance evaluation under complex and realistic urban conditions.

B. Scenarios and Parameters

This section describes the flight scenario as well as the parameters used for the communication module, perception module, and baseline methods. The simulation scenario includes a Non-Line-of-Sight (NLOS) segment and features linear flight trajectories at multiple distances. The 2D relative path and 3D trajectory are shown in Figure 5 and Figure 6, respectively. While the number of data points and the transmitter's stationary (hovering) condition remain constant, the inter-UAV distance varies, reaching up to approximately 30 m. To evaluate close-range tracking difficulty, the receiver follows straight-line segments at both short and medium distances. Even when moving at the same linear velocity, the angular rate becomes significantly higher at short distances, making accurate tracking especially challenging for the GNSS-based method. By incorporating a range of distances, this scenario effectively highlights the advantages of the proposed hybrid approach. The switching threshold is chosen based on findings from our previous work [23]. The Tx UAV hovers at 70 m while the Rx UAV flies between 69 m and 73 m. Although body blockage could occur when the Rx UAV is at a higher altitude, this study utilizes a simplified airframe model without self-shadowing to focus on validating the perception-based beam steering logic. Accounting for detailed airframe shadowing remains for future work.

In this section, we assume a millimeter-wave system operating at 60 GHz with a 16 × 16 Uniform Rectangular Array (URA) antenna. For simplicity, the number of reflections in the simulation is set to zero, meaning that multipath propagation is not considered. This assumption is reasonable because the camera-based detection range is relatively short, where the direct path dominates. Although the channel typically follows a two-ray model, the influence of scatterers diminishes as UAV altitude increases. At 60 GHz, the high attenuation further reduces the contribution of reflected components, making ground reflections negligible at short distances. The simulation uses a ray-tracing–based propagation model incorporating urban building geometries, but with reflections disabled. As a result, the channel is modeled as either a line-of-sight (LOS) link or a complete blockage by buildings, and no multipath components or delay spread are present in this evaluation.

For the perception module, we trained a tiny-yolov4-coco model using a custom dataset of 2,730 manually labeled images collected from multiple flight scenarios. The model was trained for up to 40 epochs using the Adam optimizer, with a mini-batch size of 4, an initial learning rate of 10^{-3}, and an L2 regularization factor of 5×10^{-4}. All training data were manually annotated to ensure accurate UAV detection

Fig. 5. Image from Ego UAV. The solid arrows indicates the LOS case, and the dashed arrows indicates the NLOS case.

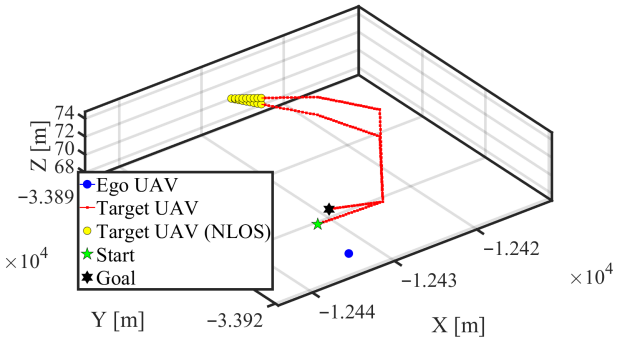

Fig. 6. 3D Trajectory.

across diverse environments. The proposed framework employs 1280×720 RGB input to generate a 2D bounding box, which defines a 3D viewing frustum. This frustum filters the LiDAR point cloud to identify the target's 3D centroid through clustering. Finally, the relative azimuth (ϕ) and elevation (θ) angles are computed from this centroid for precise beam steering.

The parameters used for the baseline methods are described as follows. For the GNSS-based baseline, we employed the built-in GPS model in MATLAB, assuming a relatively accurate receiver with horizontal and vertical positioning errors of 0.24 m and 0.45 m, respectively, and an update rate of 10 Hz. The beam-sweeping baseline adopts a hierarchical search strategy for initial link acquisition and recovery. The procedure consists of two stages: a coarse search using 12 beams with 30° spacing to cover a 90° × 60° sector, followed by a fine search using 16 beams with 10° spacing. During tracking, a more efficient local search using 9 beams with 10° spacing is applied. The threshold for declaring link loss is set to an SNR of 5 dB.

C. Processing Latency Model

To model the latency characteristics of each method, we incorporated processing delays into our 60 Hz simulation (16.7 ms per time step). The latency of the proposed Camera/LiDAR approach is based on empirical measurements: the perception stage (YOLO detection: 32.75 ms; clustering: 6.53 ms) and the beam control stage (0.02 ms) yield a total end-to-end delay of approximately 40 ms, corresponding to a 3-step latency. For the baseline methods, the codebook-based approach—whose timing is derived from the IEEE 802.11ad standard and related studies [24]—is modeled with a 106 ms latency (7-step delay)

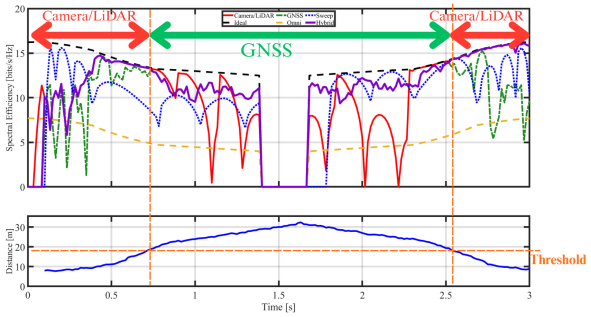

Fig. 7. Hybrid approach depending on the distance.

for initial link acquisition and a 16.7 ms latency (1-step delay) during tracking. The GNSS-based method is constrained by its 10 Hz update rate, resulting in a maximum latency of 100 ms, equivalent to a 6-step delay.

D. Communication Link Performance

First, following the findings in [23], the switching threshold for the hybrid approach is set to 19 m, based on preliminary experimental results. Figure 7 shows the system's switching behavior as a function of inter-UAV distance. Beyond 19 m, the red curve representing the Camera/LiDAR method becomes unstable due to a significant drop in detection accuracy at longer ranges. In this region, the GNSS-based method—despite its intrinsic errors—maintains relatively consistent throughput, demonstrating higher stability. Within 19 m, however, the GNSS method frequently fails to keep the target within the antenna's half-power beamwidth because its low update rate leads to substantial angular tracking errors at close range. This results in pronounced throughput degradation and fluctuations. In contrast, the Camera/LiDAR method, although showing some initial ambiguity during link establishment, achieves a throughput close to the Ideal case after approximately 2.5 s. The Beam Sweep method exhibits an oscillatory throughput pattern, primarily because it can steer only to discrete angular directions. With the narrow beamwidth used in this scenario, even small pointing errors become significant, amplifying the observed fluctuations.

Second, examining the CDF results in Figure 8, we observe that in the low-to-mid performance region, the Camera/LiDAR method shows a high cumulative probability, whereas the Hybrid method exhibits the lowest. This outcome aligns with the previous analysis: the camera's detection accuracy deteriorates substantially beyond 19 m, resulting in frequent throughput degradation. In the high-performance region, however, the Camera/LiDAR and Hybrid methods perform nearly identically. There is even a brief mid-range interval where the Camera/LiDAR method slightly outperforms the Hybrid approach. This occurs when the camera successfully detects the target at distances beyond 19 m, momentarily yielding higher throughput than the GNSS-based component of the Hybrid method. Although the GNSS method exhibits a distribution similar to the Hybrid approach, the Hybrid CDF curve is shifted further to the right because it benefits from the high-

TABLE II
COMPARISON OF RESULTS FOR EACH METHOD.

Method	Avg. Spectral Efficiency
Hybrid	10.71 bits/s/Hz
Camera/LiDAR	9.87 bits/s/Hz
GNSS-based	9.75 bits/s/Hz
Beam Sweep	9.45 bits/s/Hz
Ideal	12.71 bits/s/Hz
Omni	5.00 bits/s/Hz

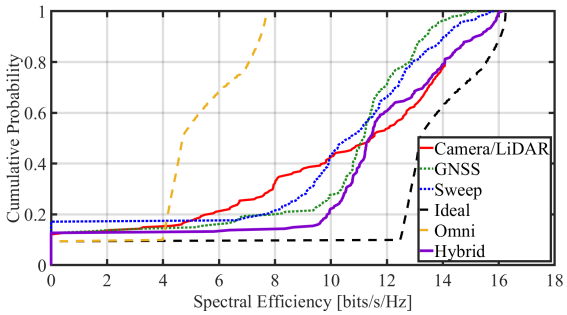

Fig. 8. CDF of Spectral Efficiency with hybrid approach.

accuracy Camera/LiDAR detection at short ranges. Overall, across a scenario spanning both short and long distances, the Camera/LiDAR method shows highly variable performance, making it unsuitable as a stable communication link. In contrast, the Hybrid method mitigates the limitations of both sensing modalities and delivers consistently high performance. As summarized in Table II, the Hybrid method achieves an average spectral efficiency that is 8.5% higher than that of the Camera/LiDAR-only method.

V. CONCLUSION

This paper presented a hybrid machine learning–supported sensor fusion system that enables resilient and high-throughput mmWave beamforming for inter-UAV communication. Starting from a link budget analysis, we demonstrated the necessity of directional antennas on both UAVs and highlighted the severe limitations caused by beam misalignment under realistic UAV mobility. To address this challenge, we developed a hybrid perception-and-tracking framework that combines the high-accuracy, low-latency Camera/LiDAR method at short range with a GNSS-based approach that is more stable at longer ranges. By dynamically switching between the two methods based on a distance threshold, the proposed system overcomes the weaknesses inherent to each individual method. Through high-fidelity co-simulation using MATLAB/Simulink and Unreal Engine with realistic urban models, the hybrid approach achieved stable performance across a wider range of distances and yielded an 8.5% improvement in average spectral efficiency compared to the Camera/LiDAR-only approach. These results demonstrate that hybrid sensing is a promising solution toward robust, autonomous, and high-data-rate inter-UAV mmWave links, enabling future applications such as distributed sensing, digital-twin data transfer, and aerial mesh networking. Future work will extend this framework to multi-UAV scenarios, dynamic threshold optimization, and real-world flight experiments.

ACKNOWLEDGMENT

This research was partially supported by JSPS KAKENHI Grant Number 25K15090.

REFERENCES

[1] G. K. Tran, M. Ozasa, and J. Nakazato, "NFV/SDN as an enabler for dynamic placement method of mmWave embedded UAV access base stations," *Network,* vol. 2, pp. 479–499, 2022.
[2] T. Sumitani and G. K. Tran, "Study on the construction of mmWave-based IAB-UAV networks," in Proc. AINTEC, Hiroshima, Japan, Dec. 19–21, 2022.
[3] A. Amrallah, E. M. Mohamed, G. K. Tran, and K. Sakaguchi, "UAV trajectory optimization in a post-disaster area using dual energy-aware bandits," Sensors, vol. 23, no. 1402, 2023.
[4] XGMF White Paper, "5G Enhancement with Millimeter Wave Deployment," ODAIBA IX Core, Jan. 2025.
[5] K. Sakaguchi, et al., "Where, When, and How mmWave is Used in 5G and Beyond," IEICE Trans. Electron. (Invited), IEICE, Vol. E100–C, No. 10, Oct. 2017.
[6] N. Okubo et al., "Field Evaluation of 5G mmWave Relays in Various Topologies: NLOS Coverage Enhancement and Tolerance Against Blockage," IEEE Access, vol. 13, pp. 77749-77763, 2025.
[7] Y. Sugimoto, G. K. Tran, "A study on visual sensors based link quality prediction for UAV-to-UAV communications,," IEICE SmartCom 2025, Jun. 2025.
[8] Beyond 5G White Paper, "Repeater, Metasurface and RIS/IRS," 6G Radio Technology Project, May 2025.
[9] Tran, G.K.; Nakazato, J.; Sou, H.; Iwamoto, H. Research on smart wireless aerial networks facilitating digital twin construction. *IEICE Trans. Commun.* **2026**, *E109-B*, 4.
[10] R. Masaoka, G. K. Tran, J. Nakazato, K. Sakaguchi, "The Future of Flying Base Stations: Empirical and Numerical Investigations of mmWave-Enabled UAVs," Future Internet 2024, 16, 5.
[11] K. Hirata, "Design of mmWave Mesh Backhaul with Drones," Master Thesis, Tokyo Institute of Technology, Mar. 2021. (in Japanese)
[12] H.T. Friis, "A Note on a Simple Transmission Formula," IRE Proc. 34 (5): 254–256. H.T. May 1946.
[13] Antenna Engineering Handbook, IEICE, pp.356-357, 1980. (in Japanese)
[14] J. Hirokawa, T. Tomura, "Millimeter-wave antennas, Antenna Engineering Handbook," McGraw-Hill Education, 5th ed., ch. 26, pp. 669-678, Dec. 2018.
[15] G. K. Tran, "A Study on Throughput Coverage Evaluation of Non-Terrestrial Communication Base Stations," ICUFN 2024, IEEE, July 2024.
[16] H. -L. Song and Y. -C. Ko, "Beam Alignment for High-Speed UAV via Angle Prediction and Adaptive Beam Coverage," in IEEE Transactions on Vehicular Technology, vol. 70, no. 10, pp. 10185-10192, Oct. 2021.
[17] J. Pokorny et al., "Concept design and performance evaluation of UAV-based backhaul link with antenna steering," in Journal of Communications and Networks, vol. 20, no. 5, pp. 473-483, Oct. 2018.
[18] T. S. Rappaport et al., "Millimeter Wave Mobile Communications for 5G Cellular: It Will Work!," in IEEE Access, vol. 1, pp. 335-349, 2013.
[19] Y. Sugimoto and G. K. Tran, "Autonomous mmWave beamforming for UAV-to-UAV communication using LiDAR–camera sensor fusion," in Proc. IEEE Global Communications Conf. (GLOBECOM), 2025.
[20] M. N. Cahyadi, T. Asfihani, H. F. Suhandri, and S. C. Navisa, "Analysis of GNSS/IMU sensor fusion at UAV quadrotor for navigation," IOP Conf. Ser. Earth Environ. Sci., vol. 1276, no. 012021, 2023.
[21] D. Lopez-Perez, I. Guvenc, and X. Chu, "Mobility management challenges in 3GPP heterogeneous networks," *IEEE Commun. Mag.,* vol. 50, pp. 70–78, 2012.
[22] K. Qi, T. Liu, and C. Yang, "Federated learning based proactive handover in millimeter-wave vehicular networks," in Proc. 15th IEEE Int. Conf. Signal Process. (ICSP), Beijing, China, Dec. 6–9, 2020, pp. 401–406.
[23] Y. Sugimoto and G.K. Tran, "Hybrid Sensor Fusion Beamforming for UAV mmWave Communication," *Future Internet,* 17(11), 521, 2025.
[24] H. Haitham, A. Omid, R. Michael, A. Mohammed, K. Dina, and I. Piotr, "Fast millimeter wave beam alignment," in Proc. ACM SIGCOMM, Budapest, Hungary, Aug. 20–25, 2018, pp. 432–445.